ARTICLE

Journal of Materials Chemistry
www.rsc.org/materials

Flat gold nanostructures by the reduction of chloroaurate ions constrained to a monolayer at the air–water interface

Anita Swami, Manasi Kasture, Renu Pasricha and Murali Sastry*

Materials Chemistry Division, National Chemical Laboratory, Pune – 411 008, India. E-mail: sastry@ems.ncl.res.in; Fax: +91 20 5893952/5893044; Tel: +91 20 5893044

Received 23rd September 2003, Accepted 22nd October 2003
First published as an Advance Article on the web 5th November 2003

Formation of flat gold nanostructures occurs by the reduction of a Langmuir monolayer of hydrophobized chloroaurate ions using anthranilic acid as a reducing agent present in the subphase. Vigorous shaking of the aqueous chloroauric acid solution with a solution of surfactant, such as octadecylamine (ODA) or benzyldimethylstearylammonium chloride (BDSAC) in chloroform results in rapid transfer of chloroaurate ions ($AuCl_4^-$) from the aqueous phase to the chloroform phase. Strong electrostatic interactions between negatively charged chloroaurate ions and cationic head groups of ODA and BDSAC molecules, making the gold ions sufficiently hydrophobic, are believed to be responsible for the transfer of $AuCl_4^-$ ions from the aqueous to the organic phase. Surface pressure–area (π–A) isotherm measurements reveal that these hydrophobized chloroaurate ions behave as amphiphilic molecules and form stable Langmuir monolayers on the acidic aqueous subphase. Spreading of hydrophobized chloroaurate ions on the surface of aqueous anthranilic acid solution results in the immobilization of $AuCl_4^-$ ions strictly at the two dimensional surface. Hence, further reduction of these $AuCl_4^-$ ions by anthranilic acid molecules from the subphase leads to the formation of highly anisotropic, flat gold nanostructures at the air–water interface. The capping of gold nanoparticles formed at the air–water interface by ODA and BDSAC enables their facile transfer as multilayers onto suitable solid substrates by the Langmuir–Blodgett (LB) technique. Multilayer Langmuir–Blodgett films were characterized by UV-vis spectroscopy, transmission electron microscopy (TEM), electron diffraction and X-ray photoelectron spectroscopy.

Introduction

Synthesis of nanoparticles over a range of chemical compositions and sizes possessing good monodispersity is an important area of research because of the size-dependent optoelectronic and physicochemical properties of nanoparticles.[1] Now it is becoming increasingly clear that the shape of nanomaterials is also an important factor affecting their electronic and chemical properties[2–5] such as catalytic activity.[6] A number of solution-based protocols are available in the literature to obtain shape control in the case of gold and silver nanoparticles. Some of the more common methods used to achieve shape control in metal nanoparticles include seeded growth,[7,8] photoreduction[9–12] or chemical reduction[13] of precursor metal ions in the presence of shape-directing surfactants and sonoelectrochemical reduction.[14] Template-based synthesis of nanoparticles such as using porous alumina,[15,16] polycarbonate membranes,[17] carbon nanotubes,[18,19] or aqueous surfactant media[9,20] to control their shape are also well known in the literature. As far as metal and semiconductor nanoparticles are concerned, most of the protocols result in predominantly rod-like nanoparticles of silver,[21,22] gold,[7,9,23] CdSe,[4] tungsten sulfide,[24] with tunable aspect ratio, and nanoprisms of silver[3]/gold[13] and CdS.[5]

Anisotropy in nanoparticles may also be introduced by synthesizing them in constrained environments[25] or at suitable interfaces.[26,27] Fendler and co-workers have shown the formation of triangular, isohedral and decahedral gold nanoparticles by chemical reduction/UV irradiation of aqueous chloroaurate ions bound to monolayers of different surfactants at the air–water interface.[26] In this case, growth of the nanoparticles proceeds into solution away from the relatively passive interface and thus leads to some anisotropy in the gold nanoparticle shape. Since these initial studies, single crystals, irregular shaped platelike crystals or multiply-twinned nanoparticles of gold have been prepared using different Langmuir–Blodgett templates by Talham and co-workers.[28] More specifically, Talham and co-workers showed the synthesis of gold nanoparticles by the photoreduction of $AuCl_4^-$ ions in Langmuir–Blodgett films prepared from amines, quaternary ammonium ions and ammonium-functionalized phospholipids. Recently, Liz-Marzan's group[13] has shown the layer-by-layer assembly of spherical and flat triangular/hexagonal gold nanoparticles with good control over interlayer interactions by depositing insulating layers of clay and/or polyelectrolytes between the gold nanoparticle layers.

Very recently, we have outlined a strategy for achieving truly two-dimensional reduction of gold ions at the air–water interface which is not possible in the Langmuir-monolayer based methods described above.[13,26–28] We have shown the formation of highly oriented, anisotropic and extremely thin gold nanosheets at the air–water interface by the spontaneous reduction of aqueous chloroaurate ions present in the subphase by hexadecylaniline Langmuir monolayers that act as reducing and anchoring agents (Scheme 1(A)).[29] This goal of achieving localized reduction of metal ions at the air–water interface may be amplified in scope if the metal ions (as opposed to the reducing Langmuir monolayer)[29] could be constrained to a monolayer on the surface of water, with reduction accomplished through the aqueous subphase (see Scheme 1(B)). In this paper, we illustrate this new approach and show the formation of highly anisotropic, flat gold nanostructures at the air–water interface by immobilizing chloroaurate ions at the interface and further reducing them with anthranilic acid present in the subphase (Scheme 1(B)). For the gold ions to be immobilized on the surface of water, they need to be rendered hydrophobic and this was accomplished by achieving their phase transfer from water to chloroform using phase-transfer

DOI: 10.1039/b311771p

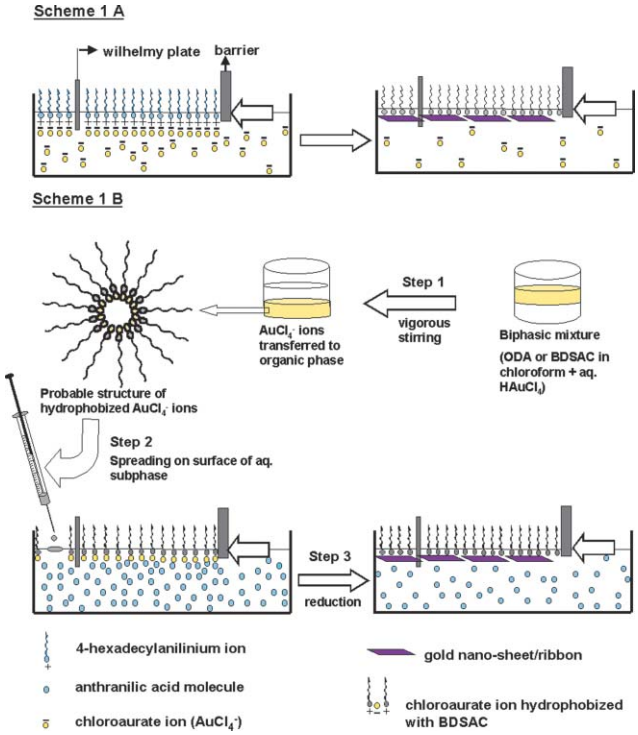

Scheme 1 (A) Diagram showing the formation of flat gold nanoribbons/nanosheets at the air–water interface by the spontaneous reduction of chloroaurate ions by a hexadecylaniline Langmuir monolayer. (B) Step 1: hydrophobization of chloroaurate ions by stirring the aqueous chloroauric acid solution with the solution of surfactants, ODA or BDSAC, in chloroform; step 2: immobilization of chloroaurate ions at the air–water interface by spreading the solution of hydrophobized chloroaurate ions on the surface of an aqueous anthranilic acid solution; step 3: formation of gold nanosheets under the monolayer by reduction of chloroaurate ions immobilized at the air–water interface using anthranilic acid solution present in the subphase as reducing agent (see text for details).

molecules such as octadecylamine (ODA) and benzyldimethylstearylammonium chloride (BDSAC, molecular structure shown in inset of Fig. 1). While phase-transfer molecules such as tetraalkylammonium salts are routinely used in the

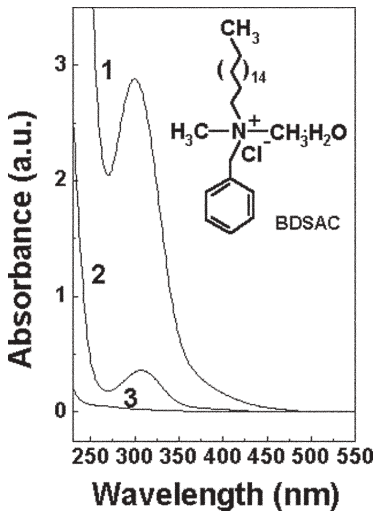

Fig. 1 UV-vis spectra of the aqueous phase of the biphasic mixture of aqueous chloroauric acid ($HAuCl_4$) and surfactant (ODA and BDSAC) in chloroform before and after the phase transfer of $AuCl_4^-$ ions from the aqueous to the organic phase. Curve 1: spectrum of the aqueous phase before phase transfer; curve 2: spectrum of the aqueous phase after phase transfer with ODA; curve 3: spectrum of the aqueous phase after phase transfer with BDSAC. The i nset shows the molecular structure of BDSAC monohydrate.

synthesis of gold nanoparticles in organic media,[30,31] to the best of our knowledge, the use of the phase-transferred hydrophobized gold ions in constrained nanoparticle growth in variable environments, such as that described in this paper, has not been described so far. The flat gold nanostructures formed at the air–water interface exhibited interesting fractal morphology and could be transferred by the Langmuir–Blodgett (LB) technique onto a variety of substrates leading to the formation of excellent multilayer films of the nanoparticles. Presented below are details of the investigation.

Experimental details

(a) Hydrophobization of chloroaurate ($AuCl_4^-$) ions

10 ml of a 1×10^{-3} M aqueous solution of chloroauric acid ($HAuCl_4$, obtained from Aldrich and used as-received) was taken in a conical flask along with a 10 ml solution of 1×10^{-3} M surfactant (ODA/BDSAC from Aldrich and used as-received) in chloroform giving immiscible layers of the colorless organic solution at the bottom of the faint yellow colored aqueous chloroauric acid solution. Vigorous stirring of the biphasic mixture facilitates electrostatic interaction between the $AuCl_4^-$ ions and the cationic head group of the surfactant, resulting in extremely rapid transfer (within 30 s) of the chloroaurate ($AuCl_4^-$) ions from the aqueous phase into the organic phase (Scheme 1(B), step 1). The organic phase containing $AuCl_4^-$ ions, which are now hydrophobic due to complexation with surfactant molecules, was separated out and diluted with chloroform to achieve a concentration of 1 mg mL^{-1} of the surfactant (ODA or BDSAC) for further experiments.

(b) Immobilization and reduction of chloroaurate ($AuCl_4^-$) ions at the air–water interface

In a typical experiment, a known volume of hydrophobized chloroaurate ions in chloroform (obtained as described above in experimental part (a); with 1 mg mL^{-1} concentration of the ODA/BDSAC) was spread on 10^{-4} M aqueous anthranilic acid (4-aminobenzoic acid, $NH_2C_6H_4COOH$, obtained from Aldrich and used as received) solution as the subphase in a Nima model 611 LB trough (Scheme 1(B), step 2). A standard Wilhelmy plate was used for surface pressure sensing. Pressure–area (π–A) isotherms were recorded at room temperature at compression and expansion rates of 50 cm^2 min^{-1} at different times after spreading the hydrophobized $AuCl_4^-$ monolayer. After measurement of the π–A isotherms, the hydrophobized chloroaurate ion monolayer was compressed to a surface pressure of 30 mN m^{-1} and maintained at this pressure for 4 h. After complete reduction of the hydrophobized chloroaurate ion Langmuir monolayer (Scheme 1(B), step 3), multilayer films of the anthranilic acid-reduced gold nanoparticles of different thickness were formed by the LB technique at a surface pressure of 25 mN m^{-1} and a deposition rate of 20 mm min^{-1} with a waiting time of 5 min between dips on quartz substrates and carbon-coated transmission electron microscopy (TEM) grids for UV-vis spectroscopy and TEM measurements, respectively. The quartz substrates were hydrophobized by depositing three monolayers of lead arachidate prior to transfer of the anthranilic acid-reduced gold nanoparticle monolayers. The hydrophobization of the support resulted in better transfer ratios of the nanoparticle monolayers. For the LB films grown on different substrates, monolayer transfer was observed both during the upward and downward strokes of the substrate at close to unity transfer ratio. UV-vis spectroscopy measurements were carried out on a JASCO dual-beam spectrophotometer (model V-570) operated at a resolution of 1 nm while TEM studies were performed using a JEOL model 1200EX instrument operated at an

accelerating voltage of 120 kV. XPS measurements on the gold nanoparticle LB films deposited on Si(111) substrates were carried out on a VG MicroTech ESCA 3000 instrument at a pressure of better than 1×10^{-9} Torr. The general scan and C 1s, N 1s and Au 4f core level spectra were recorded with unmonochromatized Mg-Kα radiation (photon energy = 1253.6 eV) at pass energy of 50 eV and electron takeoff angle (angle between electron emission direction and surface plane) of 60°. The overall resolution of measurement is thus ~1 eV for the XPS measurements. The core level spectra were background corrected using the Shirley algorithm[32] and the chemically distinct species resolved using a non-linear least squares procedure. The core level binding energies (BE) were aligned with the adventitious carbon binding energy of 285 eV.

Results and discussion

The extent of phase transfer of $AuCl_4^-$ ions from the aqueous to the organic phase by the two different surfactants, ODA and BDSAC, was measured by UV-vis spectroscopy. Fig. 1 shows the UV-vis spectra of the aqueous chloroauric acid ($HAuCl_4$) solution before and after phase transfer of $AuCl_4^-$ ions from the aqueous to organic phase while the inset shows the molecular structure of BDSAC monohydrate. Curve 1 is the spectrum of the aqueous phase before phase transfer while curves 2 and 3 correspond to the spectra of the aqueous phase after phase transfer with ODA and BDSAC, respectively. An intense resonance at 300 nm due to absorption by the Au^{3+} ions[33] is observed in curve 1. Significant reduction in intensity of this absorption band after vigorous shaking of the biphasic mixture (curves 2, 3) indicates phase transfer of $AuCl_4^-$ ions from the aqueous to chloroform phase. Simple back-of-the-envelope calculations (within the accuracy limits of absorption spectroscopy) show that 88 and 99% of $AuCl_4^-$ ions have been transferred into the chloroform phase using ODA and BDSAC as phase transfer agents, respectively. Amine groups of the ODA molecules are protonated at the pH of chloroauric acid solution (pH 3.7) and thus complex electrostatically with the $AuCl_4^-$ ions during vigorous stirring of the biphasic mixture of aqueous chloroauric acid and ODA in chloroform. This results in the $AuCl_4^-$ ions bound to the ODA molecules becoming sufficiently hydrophobic and amenable to transfer into chloroform. In the case of phase transfer of gold ions with BDSAC, electrostatic interactions between the surfactant and the gold ions are expected to be stronger due to the cationic quaternary ammonium head groups of BDSAC molecules, thereby leading to a larger percentage (99%) of $AuCl_4^-$ ions transferred into the organic phase. Thus, UV-Vis spectroscopic measurements indicate that the phase transfer of $AuCl_4^-$ ions from the aqueous to the organic phase is more facile using BDSAC than ODA as a phase transfer agent. We believe that the gold ions are entrapped along with the surfactant in the form of micelles. Even though most studies on the synthesis of gold nanoparticles in organic solvents use phase transfer molecules similar to those used in this study (the Brust method),[30] to the best of our knowledge, the exact nature of the gold ion-phase transfer molecule complex in the organic phase prior to metal ion reduction is poorly understood.

Surface pressure–area (π–A) isotherm measurements were performed to check the ability of surfactant molecules now complexed with $AuCl_4^-$ ions (ODA^+–$AuCl_4^-$ and $BDSA^+$–$AuCl_4^-$) to form stable Langmuir monolayers on an aqueous subphase. In Fig. 2(A) and (B), curve 1 shows the π–A isotherm cycle of ODA^+–$AuCl_4^-$ and $BDSA^+$–$AuCl_4^-$, respectively, on the surface of acidic water (pH 4.5) recorded 1 h after spreading the monolayers. Curves 2, 3 and 4 in Fig. 2(A) and (B) likewise correspond to π–A isotherms recorded from ODA^+–$AuCl_4^-$ and $BDSA^+$–$AuCl_4^-$ monolayers on the surface of a 10^{-4} M aqueous anthranilic acid subphase recorded at 0, 1 and 3 h after

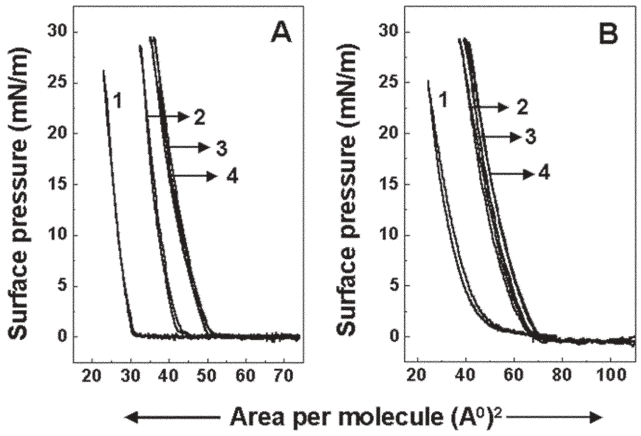

Fig. 2 (A) Curve 1: π–A isotherm during one compression and expansion cycle of ODA electrostatically complexed with chloroauric acid ($HAuCl_4$) on acidic water (pH 4.5) subphase recorded 1 h after spreading the monolayer. Curves 2, 3, 4 : π–A isotherms of ODA^+–$AuCl_4^-$ on 10^{-4} M aqueous anthranilic acid subphase recorded 0, 1 and 3 h after spreading the monolayer, respectively. (B) Curve 1: π–A isotherm during one compression and expansion cycle of benzyldimethylstearylammonium chloride (BDSAC) electrostatically complexed with chloroauric acid ($HAuCl_4$) on acidic water (pH 4.5) subphase recorded 1 h after spreading the monolayer. Curves 2, 3, 4: π–A isotherms of $BDSA^+$–$AuCl_4^-$ on 10^{-4} M aqueous anthranilic acid subphase recorded 0, 1 and 3 h after spreading the monolayer, respectively.

spreading the monolayers, respectively. A steep build up in surface pressure in both cases up to 30 mN m^{-1} indicates that the ODA^+–$AuCl_4^-$ and $BDSA^+$–$AuCl_4^-$ form stable monolayers on both acidic water (pH 4.5) and anthranilic acid as the subphase (Fig. 2(A) and (B)). This clearly indicates that in case of both acidic water (pH 4.5) and anthranilic acid subphase, ODA^+–$AuCl_4^-$ and $BDSA^+$–$AuCl_4^-$ behave like classical amphiphiles, wherein the hydrophilic $AuCl_4^-$ ions complexed with the hydrophobic surfactant molecules anchors the complex to the subphase. It is likely that the micellar structure of the ODA^+–$AuCl_4^-$ and $BDSA^+$–$AuCl_4^-$ complexes, once spread on the surface of water/anthranilic acid, is disrupted resulting in the formation of a gold ion–surfactant monolayer on the subphase (Scheme 1(B), step 2). It is important to note that the take-off molecular area of the ODA^+–$AuCl_4^-$ monolayer on the anthranilic acid subphase (50 $Å^2$ $molecule^{-1}$) recorded immediately after spreading the monolayer (Fig. 2(A), curve 2) is much higher than that recorded for this Langmuir monolayer on acidic water (pH 4.5) subphase (32 $Å^2$ $molecule^{-1}$, Fig. 2(A), curve 1). A similar increase in take-off area from 50 to 70 $Å^2$ $molecule^{-1}$ is observed in the case of the $BDSA^+$–$AuCl_4^-$ monolayer on changing the subphase from acidic water (pH 4.5) to aqueous anthranilic acid solution (Fig. 2(B), curves 1 and 2, respectively). This clearly indicates that anthranilic acid molecules present in the subphase interact strongly with the ODA^+–$AuCl_4^-$ and $BDSA^+$–$AuCl_4^-$ monolayers. It is also observed that there is a small increase in the molecular take-off area in the π–A isotherms of the ODA^+–$AuCl_4^-$ and $BDSA^+$–$AuCl_4^-$ monolayers on the anthranilic acid subphase with time (Fig. 2(A) and (B), curves 2, 3 and 4) This suggests that anthranilic acid molecules present in the subphase are very easily accessible to the $AuCl_4^-$ ions (which are bound to the surfactant monolayer and thus localized at the interface) and reduce them extremely rapidly. The process of reduction of the gold ions by anthranilic acid in the subphase could be observed by the appearance of a faint violet color at the interface that is characteristic of gold nanostructures. Since the gold ions are constrained to a monolayer at the air–water interface by the new strategy outlined above, we anticipate that reduction of these highly

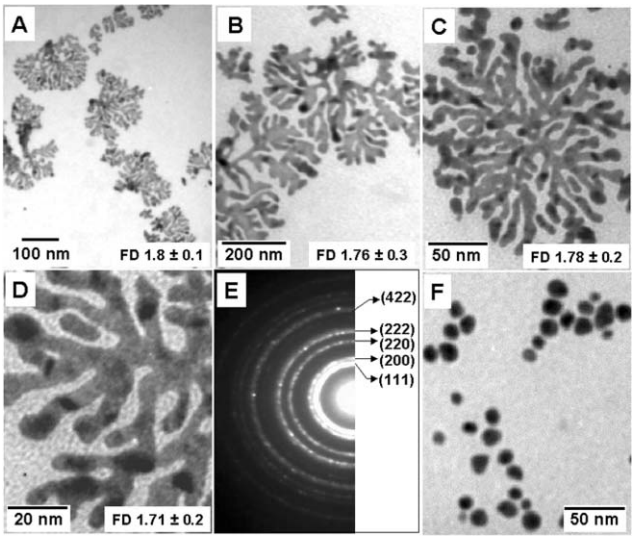

Fig. 3 (A)–(D) Representative TEM images of gold nanostructures formed at the air–water interface by the reduction of $AuCl_4^-$ ions (which are immobilized on the surface of the 10^{-4} M aqueous anthranilic acid subphase by complexing with ODA) using anthranilic acid as a reducing agent present in the subphase, recorded at different magnifications. Respective fractal dimensions are shown in the images. (E) Electron diffraction pattern recorded from flat gold nanostructures shown in image (D). (F) TEM image of gold nanoparticles formed at the liquid–liquid interface by the reduction of hydrophobic $AuCl_4^-$ ions (hydrophobized by complexing with ODA) in chloroform using 10^{-3} M aqueous anthranilic acid solution as a reducing agent present in the biphasic mixture.

localized ions would result in a high degree of anisotropy in the shape of the gold nanostructures formed.

The morphology of anthranilic acid-reduced gold nanostructures formed at the air–water interface was studied by depositing a one monolayer LB film of the nanoparticles on carbon-coated TEM grids. Figs. 3(A)–(D) and 4(A)–(C) show representative TEM images of anthranilic acid-reduced gold nanoparticles obtained from the ODA^+–$AuCl_4^-$ and $BDSA^+$–$AuCl_4^-$ Langmuir monolayers, respectively, at different magnifications. In both cases, assemblies of gold nanostructures are observed

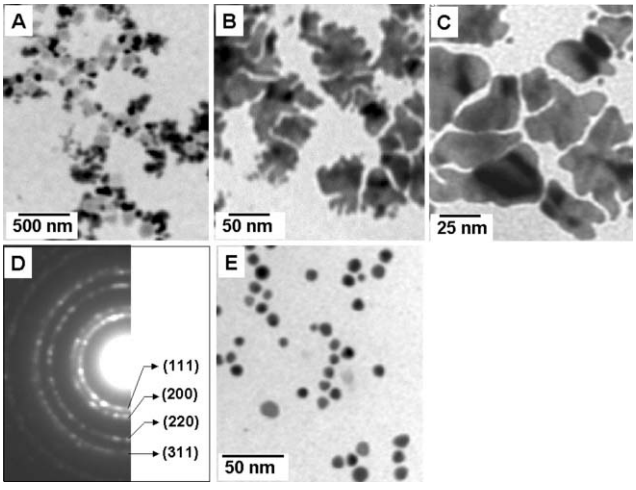

Fig. 4 (A)–(C) TEM images of gold nanostructures formed at the air–water interface by the reduction of $AuCl_4^-$ ions (which are immobilized on the surface of the 10^{-4} M aqueous anthranilic acid subphase by complexing with BDSAC) using anthranilic acid as a reducing agent present in the subphase, recorded at different magnifications. (D) Electron diffraction pattern recorded from flat gold nanostructure shown in image (C). (E) TEM image of the gold nanoparticles formed at the liquid–liquid interface by the reduction of hydrophobic $AuCl_4^-$ ions (hydrophobized by complexing with BDSAC) in chloroform using 10^{-3} M aqueous anthranilic acid solution as a reducing agent present in the biphasic mixture.

uniformly over the surface of the TEM grid at low magnification (Figs. 3(A) and 4(A)). The higher magnification images (Figs. 3(B)–(D), 4(B) and 4(C)) reveal that the gold nanostructures obtained from both ODA^+–$AuCl_4^-$ and $BDSA^+$–$AuCl_4^-$ Langmuir monolayers are highly anisotropic, flat and irregular in shape and size. Closer examination reveals that there are remarkable differences between the gold nanostructures obtained using ODA and BDSAC as complexation agents. An important and fascinating feature of the gold nanostructures obtained by reduction of the ODA^+–$AuCl_4^-$ monolayer is that they show a high frequency of fractal, dendritic structures of nanoscale dimensions extending to lengths of up to 200 nm (Fig. 3(A)–(D)). Fractal dimensions of a number of nanostructures in these images were determined and were found to vary from 1.71 ± 0.2 to 1.8 ± 0.1. Fractal dimensions have been calculated using the radial mass distribution method. In this calculation scheme, the number of pixels (picture elements) $N(R)$ in a given radius R is measured. Since for a growing fractal, $N(R) \sim R^D$, a plot of $\ln N(R)$ *vs.* $\ln R$ results in a curve which has an asymptotic slope equal to the fractal dimension, D.[34] The error in the fractal dimension is essentially the error in the slope of the asymptotic line. The slope in the $\ln N(R)$ *vs.* $\ln R$ plot was determined by the method of least squares. Formation of silver and gold fractal structures have been observed in solution under sonochemical[35] or ultrasonic agitation[36,37] and in the presence of specific surface modifiers.[38–40] Very recently, formation of fractal gold nanostructures by the spontaneous reduction of chloroaurate ions entrapped in thermally evaporated hexadecylaniline thin films due to diffusion limited aggregation has been demonstrated in this laboratory.[41] The gold fractal nanostructures obtained in this study are characteristic of diffusion-limited aggregated (DLA) structures.[42] Indeed, the fractal dimensions of the gold nanostructures obtained by reduction of ODA^+–$AuCl_4^-$ monolayers in the present study (1.7–1.8; Fig. 3(A)–(D)) are in the range expected for DLA structures (<2).[42,43] While the exact mechanism leading to formation of the fractal gold nanoparticles is not clear at the moment, we believe that the strong binding of the ODA molecules with the gold nanoparticle surface (since chloroaurate ions are hydrophobized with ODA before spreading on surface of aqueous subphase) may be partly responsible for this. While highly flat gold nanosheets of size ranging from 10 to 100 nm are obtained by reduction of the $BDSA^+$–$AuCl_4^-$ monolayer at the air–water interface (Fig. 4(B) and (C)), they do not demonstrate the same fractal structure observed in the ODA films. Figs. 3(E) and 4(D) show electron diffraction patterns recorded from the flat gold nanostructures shown in Figs. 3(D) and 4(C), respectively. It is clear from the electron diffraction pattern that the gold nanostructures formed using both ODA and BDSAC are polycrystalline in nature. The characteristic rings in the polycrystalline diffraction pattern could be indexed as the (111), (200), (220) and (311) allowed reflections from fcc gold. In order to confirm that the formation of flat, anisotropic nanostructures at the air–water interface is really a consequence of localization of gold ions at the two-dimensional surface, control experiments were performed wherein chloroaurate ions ($AuCl_4^-$ ions) hydrophobized with ODA and BDSAC are reduced in solution (at the liquid–liquid interface) using 10^{-3} M aqueous anthranilic acid solution under constant stirring for 1 h. Spherical particles with sizes ranging from 10 to 20 nm are obtained (Figs. 3(F) and 4(E)) that show a completely different morphology from that obtained at the air–water interface (Figs. 3(D) and 4(C)). The control experiments thus ensure that the flat, anisotropic nature of nanostructures formed at the air–water interface is really the result of immobilization of gold ions at the air–water interface and the highly localized reduction of these constrained ions.

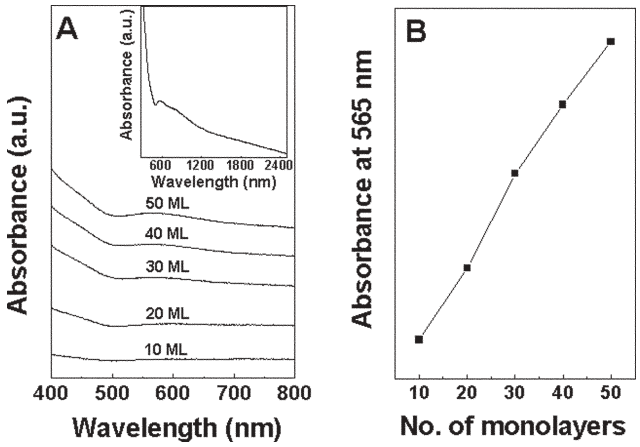

Fig. 5 (A) UV-vis spectra of LB films of gold nanoparticles deposited on a quartz substrate formed at the air–water interface by the reduction of chloroaurate ($AuCl_4^-$) ions (which are immobilized at the air–water interface using octadecylamine, ODA) using 10^{-4} M anthranilic acid as a reducing agent present in the subphase, recorded as a function of number of monolayers in the LB films. The number of monolayers of the gold nanoparticles in the LB films is indicated next to the respective curves. The inset is the the UV-vis spectrum of a 50 ML gold nanoparticle LB film recorded in the spectral range 280–2500 nm on quartz. (B) A plot of intensity of the surface plasmon resonance (absorbance at 565 nm) as a function of number of monolayers of anthranilic acid-reduced gold nanoparticle LB films grown on a quartz substrate.

One of the important advantages of the Langmuir–Blodgett (LB) technique is that it permits the characterization and utilization of nanoparticles and nanoparticulate films in the solid state by enabling their transfer onto solid substrates at any stage of their growth. Multilayer LB films of anthranilic acid-reduced gold nanoparticles were deposited on quartz substrates by the LB technique to study their optical properties. Figs. 5(A) and 6(A) show the UV-vis spectra of LB films of gold nanostructures of different thicknesses obtained by reduction of ODA^+–$AuCl_4^-$ and $BDSA^+$–$AuCl_4^-$ monolayers, respectively (the number of monolayers in the films is indicated next to the respective curves). Broad absorption bands centered at *ca.* 565 and 590 nm are observed in these two cases, that increase in intensity with increasing number of monolayers in the LB film. The absorption bands at 565 and 590 nm are due to excitation of surface plasmon vibrations in gold nanoparticles and are responsible for the characteristic pink/violet color of gold nanoparticle solutions/films.[44,45] Well-dispersed, spherical gold nanoparticles in solution usually show a sharp surface plasmon resonance at 510–530 nm. The shift and broadening of the resonance in the LB films indicates considerable aggregation and anisotropy of the particles and thus supports the TEM results. The absorptions at 565 and 590 nm increase linearly with film thickness (Figs. 5(B) and 6(B)) clearly indicating that the gold nanoparticle multilayers grow without change in nanoparticle density in successive layers even up to 60 monolayers thickness. The insets of Figs. 5(A) and 6(A) show the UV-vis spectra of a 60 ML thick LB film obtained from the ODA^+–$AuCl_4^-$ and $BDSA^+$–$AuCl_4^-$ complexes, respectively, in the spectral range 280–2500 nm. A very broad absorption is observed that interestingly extends to the near infrared region. The large absorption in the near IR is clearly a consequence of high anisotropy in the gold nanostructures in the superlattice films.

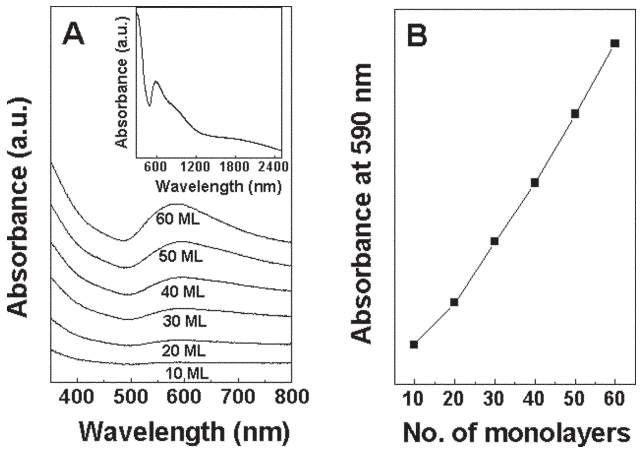

Fig. 6 (A) UV-vis spectra of LB films of gold nanoparticles deposited on a quartz substrate formed at the air–water interface by the reduction of chloroaurate ($AuCl_4^-$) ions (which are immobilized at the air–water interface using benzyldimethylstearyammonium chloride, BDSAC) by 10^{-4} M anthranilic acid as a reducing agent present in the subphase, recorded as a function of number of monolayers. The number of monolayers of the gold nanoparticles in the LB films is indicated next to the respective curve. The inset is the the UV-vis spectrum of 60 ML LB film recorded in the spectral range 280 to 2500 nm. (B) A plot of intensity of the surface plasmon resonance (absorbance at 590 nm) plotted as a function of number of monolayers of anthranilic acid-reduced gold nanoparticle LB films grown on a quartz substrate.

A 60 ML anthranilic acid-reduced gold nanoparticle film obtained by reduction of $BDSA^+$–$AuCl_4^-$ monolayers was deposited on a Si(111) substrate and analyzed by XPS. The general scan spectra of the LB film showed the presence of strong C 1s, N 1s and Au 4f core levels with no evidence of impurities. The film was sufficiently thick and therefore, no signal was measured from the substrate (Si 2p core level). The Au 4f, C 1s and N 1s core levels recorded from the film are shown in Fig. 7(A), (B) and (C), respectively. The spectra have been background corrected using the Shirley algorithm[32] prior to curve resolution. The Au 4f core level spectrum recorded from the LB film (Fig. 7(A)) could be stripped into two spin–orbit pairs (splitting 3.7 eV). Two chemically distinct Au $4f_{7/2}$ components are observed at 83.8 and 85.8 eV binding energies (BEs, labelled 1 and 2 in Fig. 7(A)). The lower BE component is attributed to electron emission from Au metal in the LB film while the high BE component arises from unreduced Au^{3+} ions in the LB film[31] indicating that a small fraction of the $AuCl_4^-$ ions remain in the film. The C 1s core level spectrum recorded from the LB film could be stripped into four components at 282.2, 284.9, 286.5 and 288.4 eV (Fig. 7(B)) indicating the presence of four chemically distinct carbons in the film. The high BE component observed at 288.4 eV can be assigned to the carbon bonded to oxygen in the carboxylic group of anthranilic acid which is also observed in the C 1s core level spectrum recorded from the drop-coated film of an aqueous solution of only anthranilic acid (data not shown). The 286.5 eV BE peak is attributed to the carbon adjacent to the carboxylic acid group in anthranilic acid. Two chemically distinct

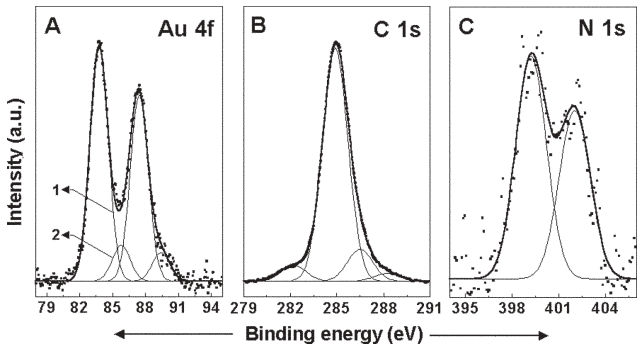

Fig. 7 (A) Au 4f, (B) C 1s and (C) N 1s core level spectra recorded from a 60 ML anthranilic acid-reduced gold nanoparticle film at the air–water interface deposited on a Si(111) substrate 4 h after spreading the monolayer of BDSAC complexed with chloroaurate ions on a 10^{-4} M anthranilic acid subphase. The solid lines are non-linear least square fits to the data.

components are observed at 399.2 and 402 eV in the case of the N 1s core level spectrum (Fig. 7(C)). The presence of two N 1s signals also supports the presence of anthanilic acid in the LB film along with the hydrophobizing agent, BDSAC.

In summary, we have shown that chloroaurate ions can be easily immobilized at the air–water interface by rendering them hydrophobic. This is accomplished by complexing them with surfactants such as octadecylamine and benzyldimethylstearylammonium chloride at the liquid–liquid interface and facilitating their phase transfer into chloroform. Further reduction of these chloroaurate ions constrained to a monolayer at the air–water interface by anthranilic acid present in the subphase results in the formation of highly anisotropic, flat gold nanostructures at the interface. These nanostructures can be transferred onto suitable solid substrates in a lamellar fashion to form superlattice films of desired thickness using the elegant LB technique.

Acknowledgements

A. S. would like to thank the Council for Scientific and Industrial Research (CSIR), Govt. of India, for a research fellowship. The Center for Materials Characterization (CMC), NCL Pune is acknowledged for assistance with the XPS analysis. This work was partially funded by a grant to M. S. from the Department of Science and Technology (DST), Govt. of India and is gratefully acknowledged. We thank Dr Arun Banpurkar, Department of Physics, University of Pune, for the fractal dimension calculations.

References

1 G. Schmid, *Chem. Rev.*, 1992, **92**, 1709.
2 M. El-Sayed, *Acc. Chem. Res.*, 2001, **34**, 257.
3 R. Jin, Y.-W. Cao, C. A. Mirkin, K. L. Kelly, G. C. Schatz and J. G. Zheng, *Science*, 2001, **294**, 1901.
4 X. Peng, L. Manna, W. Yang, J. Wickham, E. Scher, A. Kadanavich and A. P. Alivisatos, *Nature*, 2000, **404**, 59.
5 N. Pinna, K. Weiss, J. Urban and M.-P. Pileni, *Adv. Mater.*, 2001, **13**, 261.
6 T. S. Ahmadi, Z. L. Wang, T. C. Green, A. Henglein and M. A. El-Sayed, *Science*, 1996, **272**, 1924.
7 K. R. Brown, D. C. Walter and M. Natan, *Chem. Mater.*, 2000, **12**, 306.
8 N. R. Jana, L. Gearheart and C. J. Murphy, *J. Phys. Chem. B*, 2001, **105**, 4065.
9 K. Esumi, K. Matsuhisa and K. Torigoe, *Langmuir*, 1995, **11**, 3285.
10 A. Kameo, A. Suzuki, K. Torigoe and K. Esumi, *J. Colloid Interface Sci.*, 2001, **241**, 289.
11 E. Leontidis, K. Kleitou, T. Kyprianidou-Leodidou, V. Bekiari and P. Lianos, *Langmuir*, 2002, **18**, 3659.
12 Y. Zhou, C. Y. Wang, Y. R. Zhu and Z. Y. Chen, *Chem. Mater.*, 1999, **11**, 2310.
13 N. Malikova, I. Pastoriza-Santos, M. Scheirhorn, N. A. Kotov and L. M. Liz-Marzan, *Langmuir*, 2002, **18**, 3694.
14 Z. Zhu, S. Liu, O. Palchik, Y. Koltypin and A. Gedanken, *Langmuir*, 2000, **16**, 6396.
15 B. R. Martin, D. J. Dermody, B. D. Reiss, M. M. Fang, L. A. Lyon, M. J. Natan and T. E. Mallouk, *Adv. Mater.*, 1999, **11**, 1021.
16 B. M. I. van der Zande, M. R. Bohmer, L. G. Fokkink and C. Schonenberger, *Langmuir*, 2000, **16**, 451.
17 V. M. Cepak and C. R. Martin, *J. Phys. Chem. B*, 1998, **102**, 9985.
18 A. Govindaraj, B. C. Satishkumar, M. Nath and C. N. R. Rao, *Chem. Mater.*, 2000, **12**, 202.
19 S. Fullam, D. Cottell, H. Rensmo and D. Fitzmaurice, *Adv. Mater.*, 2000, **12**, 1430.
20 Y. Y. Yu, S. S. Chang, C. L. Lee and C. R. C. Wang, *J. Phys. Chem.*, 1997, **101**, 6661.
21 S.-W. Chung, G. Markovich and J. R. Heath, *J. Phys. Chem. B.*, 1998, **102**, 6685.
22 N. R. Jana, L. Gearhart and C. J. Murphy, *Chem. Commun.*, 2001, 617.
23 C. J. Johnson, E. Dujardin, S. A. Davis, C. J. Murphy and S. Mann, *J. Mater. Chem.*, 2002, **12**, 1765.
24 S. I. Nikitenko, Y. Koltypin, Y. Mastai, M. Koltypin and A. Gedanken, *J. Mater. Chem.*, 2002, **12**, 1450.
25 J. K. Pike, H. Byrd, A. A. Morrone and D. R. Talham, *J. Am. Chem. Soc.*, 1993, **115**, 8497.
26 K. C. Yi, V. S. Mendieta, R. L. Castanares, F. C. Meldrum, C. Wu and J. H. Fendler, *J. Phys. Chem.*, 1995, **99**, 9869.
27 J. H. Fendler and F. C. Meldrum, *Adv. Mater.*, 1995, **7**, 607.
28 S. Ravaine, G. E. Fanucci, C. T. Seip, J. H. Adair and D. R. Talham, *Langmuir*, 1998, **14**, 708.
29 A. Swami, A. Kumar, P R. Selvakannan, S. Mandal, R. Pasricha and M. Sastry, *Chem. Mater.*, 2003, **15**, 17.
30 M. Brust, M. Walker, D. Bethell, D. J. Schiffrin and R. Whyman, *J. Chem. Soc., Chem. Commun.*, 1994, 801.
31 D. V. Leff, L. Brandt and J. R. Heath, *Langmuir*, 1996, **12**, 4723.
32 D. A. Shirley, *Phys. Rev. B.*, 1972, **5**, 4709.
33 A. Henglein, *Langmuir*, 1999, **15**, 6738.
34 T. Vicsek, *Fractal Growth Phenomena*, World Scientific, Singapore, 2nd edn., 1992.
35 S. I. Nikitenko, Y. Koltypin, Y. Mastai, M. Koltypin and A. Gedanken, *J. Mater. Chem.*, 2002, **12**, 1450.
36 J. Xiao, Y. Xie, R. Tang, M. Chen and X. Tian, *Adv. Mater.*, 2001, **13**, 1887.
37 J. Zhu, X. Liao and H-Y. Chen, *Mater. Res. Bull.*, 2001, **36**, 1687.
38 Y. Zhou, S. H. Yu, C. Y. Wang, X. G. Li and Y. R. Z. Y. Zhu Chen, *Adv. Mater.*, 1999, **11**, 850.
39 Wang X., K. Naka, H. Itoh, S. Park and Y. Chujo, *Chem. Commun.*, 2002, 1300.
40 S. T. Selvan, *Chem. Commun.*, 1998, 351.
41 S. Mandal, S. Phadtare, P. R. Selvakannan, R. Pasricha and M. Sastry, *Nanotechnology*, 2003, **14**, 878.
42 M. Y. Lin, H. M. Lindsay, D. A. Weitz, R. C. Ball, R. Klein and P. Meakin, *Nature*, 1989, **339**, 360.
43 K. Solecka-Cermakova, B. Vlckova and F. Lednicky, *J. Phys. Chem.*, 1996, **100**, 4954.
44 A. Henglein, *J. Phys. Chem.*, 1993, **97**, 5457.
45 K. S. Mayya, V. Patil and M. Sastry, *Langmuir*, 1997, **13**, 2575.